



# Feasibility of Seismic Monitoring at a Potential CO<sub>2</sub> Injection Test Site in the Paris Basin

Marc Becquey, N. Lucet, F. Huguet

## ► To cite this version:

Marc Becquey, N. Lucet, F. Huguet. Feasibility of Seismic Monitoring at a Potential CO<sub>2</sub> Injection Test Site in the Paris Basin. Oil & Gas Science and Technology - Revue d'IFP Energies nouvelles, 2010, 65 (4), pp.589-595. 10.2516/ogst/2009033 . hal-01937550

HAL Id: hal-01937550

<https://ifp.hal.science/hal-01937550>

Submitted on 2 Jan 2019

**HAL** is a multi-disciplinary open access archive for the deposit and dissemination of scientific research documents, whether they are published or not. The documents may come from teaching and research institutions in France or abroad, or from public or private research centers.

L'archive ouverte pluridisciplinaire **HAL**, est destinée au dépôt et à la diffusion de documents scientifiques de niveau recherche, publiés ou non, émanant des établissements d'enseignement et de recherche français ou étrangers, des laboratoires publics ou privés.

# Feasibility of Seismic Monitoring at a Potential CO<sub>2</sub> Injection Test Site in the Paris Basin

M. Becquey<sup>1</sup>, N. Lucet<sup>1</sup> and F. Huguet<sup>2</sup>

<sup>1</sup> Institut français du pétrole, IFP, 1-4 avenue de Bois-Préau, 92852 Rueil-Malmaison Cedex - France

<sup>2</sup> GDF-Suez, 361 avenue du Président Wilson, 93200 Saint-Denis - France

e-mail: marc.becquey@ifp.fr - nathalie.lucet@beicip.fr - frederic.huguet@gazdefrance.com

**Résumé — Évaluation des apports de la sismique à la surveillance d'un test d'injection de CO<sub>2</sub> sur un site pilote potentiel du Bassin de Paris** — Les effets sismiques de l'injection de dioxyde de carbone dans un gisement de pétrole déplété ont fait l'objet d'une simulation. Ces effets sont faibles. On peut s'attendre à une variation des temps d'arrivée des réflexions sur des interfaces situées en dessous des réservoirs, de l'ordre de la demi-milliseconde, et à une variation d'amplitude au toit et au mur du réservoir de l'ordre de 6 %. La variation d'amplitude sera légèrement plus forte pour les réflexions à grand déport, mais le pointé des réflexions et la mesure des amplitudes seront probablement plus difficiles, en raison de la présence d'ondes converties. La mesure de l'anisotropie azimutale, due à la présence de fractures, peut nous donner des informations sur l'état de fracturation du réservoir et sur la connexion entre ces fractures et la matrice poreuse. La mesure de ces variations subtiles nécessitera une acquisition soignée et un traitement précautionneux des données.

**Abstract — Feasibility of Seismic Monitoring at a Potential CO<sub>2</sub> Injection Test Site in the Paris Basin** — Seismic effects of the injection of CO<sub>2</sub> into a partially depleted oil field have been evaluated. Seismic modelling yields small time-lapse effects, including 0.4 ms time-shifts and 4 to 6% amplitude variations at the top and bottom of the reservoir. Amplitude variations at the reservoir level should be slightly larger at large incidence angles, but wave equation modelling shows that picking these reflections will not be easy, because of the presence of shear waves generated at upper interfaces. In-situ fracturation generates azimuthal anisotropy with velocity and amplitude variations with the propagation direction. These variations bear some information about the crack density, about the relation between the fracture nets and the porous medium, and about the fluid content in the pores and fractures. All these effects are however weak and their measurement requires careful seismic data acquisition and processing.

## INTRODUCTION

Some potential targets have been selected in the Paris Basin for the purpose of geological storage of carbon dioxide. Among them, an oil reservoir at a depth of 1450 m in the Dogger limestones. Is it possible to follow the displacement of the carbon dioxide injected into the reservoir and to detect possible leakage by seismic monitoring? The storage reservoir being made of stiff and not very porous rocks, the efficiency of seismic techniques was to be tested, taking account of the information available.

## 1 MODELLING THE INJECTION

The oil reservoir, selected as a test site for an integrated study about geological CO<sub>2</sub> storage by the PICOREF programme (Brosse *et al.*, this issue), exhibits an anticline structure, with oil/water contact about 60 meters under the top. It includes four units, with porosities ranging from 8 to 13%. The average permeability is 10 mD.

A full set of logs, allowing a confident determination of the lithology, was available for one well only. In four other wells, all located, as the former, in the north-eastern fourth of the structure, gamma-ray and sonic logs only were available. Hence it was not possible to build a complete geological and petrophysical model of the structures.

A learning process was applied to the first well, in order to establish correlations between the lithological composition

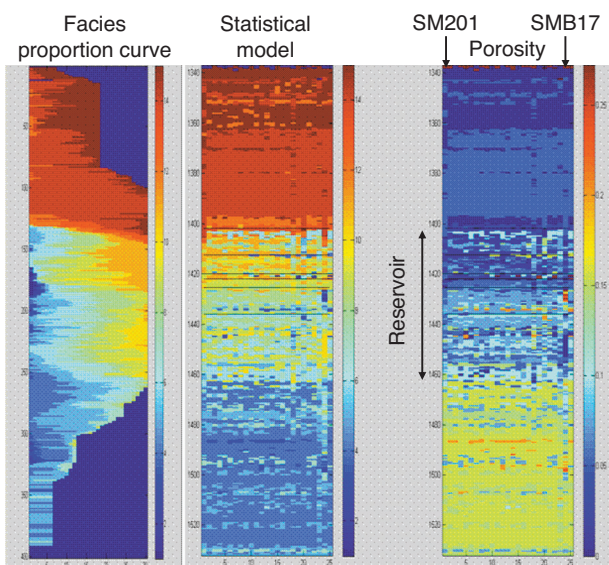


Figure 1

Facies proportion curve and statistical model at the left. Low permeability limestones in dark blue, reservoir limestones in light blue, tight limestones in orange, shales in red. Resulting porosity at the right.

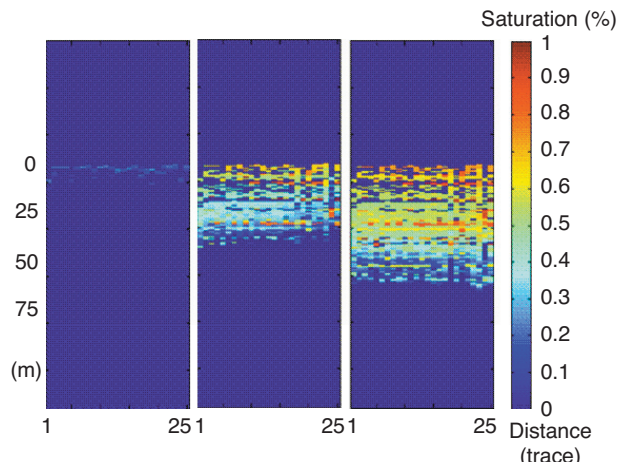


Figure 2  
CO<sub>2</sub> injection simulation.  
Beginning, mid-term and end of injection period.

and the gamma-ray and sonic logs. The porosity and the shale to limestone ratio were estimated for the five wells on the basis of these correlations. A series of 15 facies was determined, ranging from porous limestones to shales, and a vertical facies proportion curve was computed. Porosities, permeabilities, input pressure and capillary pressure curves were associated with each of these facies. A geological and petrophysical 2-D 25-column model was designed, including the five wells and 20 pseudo-wells, obtained by statistical variations around the vertical facies proportion curve (Fig. 1).

A simulation of the injection was performed, step by step, with a progressive filling of the reservoir. The injection was stopped when an incremental pore pressure of 1.5 MPa was reached at the injection point.

Figure 2 displays the CO<sub>2</sub> saturation at the beginning and at the end of the injection and at a mid-term step.

Figure 3 displays at a given position the progressive filling over the whole period of injection. The injected CO<sub>2</sub> appears first at the top of the uppermost reservoir and progressively fills a larger height in the reservoir zone, until it reaches the oil/water contact at the end of the injection.

The local saturation was computed using the capillarity pressure curves.

The average saturation in the reservoir zone was about 50%. A maximum of about 95% is reached in karstified zones.

The properties of the fluids were inferred from their known composition: the oil/water mix in place has a density of 950 kg/m<sup>3</sup> and a bulk modulus of about 1 GPa. The density of the injected carbon dioxide, at a pore pressure ranging between 14.4 and 15.9 MPa and at a temperature of 63°C, is equal to 550 kg/m<sup>3</sup> and its bulk modulus is about 0.45 GPa. The P-wave velocity in the reservoir was computed from the

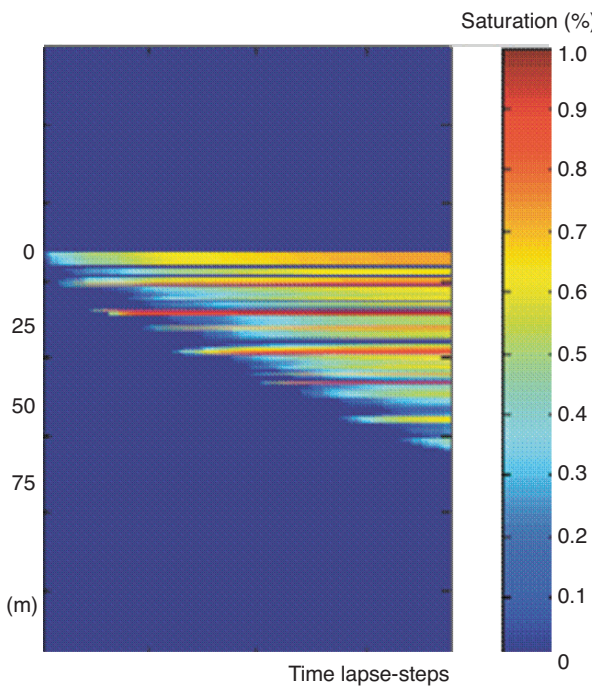


Figure 3  
Evolution of CO<sub>2</sub> saturations during the injection period at a given position.

stages of the injection, up to step 20, only one event is visible, the reflections at the top and at the bottom of the CO<sub>2</sub>-invaded zone interfering and giving rise to the so-called “tuning effect”. After some time, around step 25, the two reflections separate and can be distinguished. Their amplitude does not exceed 5 to 6% of the amplitude of the reflection at the top of the uppermost reservoir before the beginning of the injection. The tuning effect at the first steps can however raise the amplitude difference up to about 10% of the initial amplitude. Reflections from beneath the reservoir zone are shifted in time with respect to the pre-injection trace by an increment that increases progressively, reaching  $0.45 \pm 0.05$  ms at the end of the injection period. The time shift is strongly correlated and almost proportional to the height of the column where CO<sub>2</sub> is present, whatever the saturations.

Experience acquired from time-lapse acquisition and processing suggests that we should be able to detect and measure a 0.2 ms time shift and a difference in amplitude of 20% for surface monitoring, a 0.1 ms time shift and a 10% amplitude difference using permanent emission and reception systems. Under these conditions, the time-shift and hence the height of the column where some CO<sub>2</sub> is present, should be measurable. Access to the amplitude difference seems at the very limit of the capacities of time lapse land seismics.

facies composition, taking the saturation into account using Gassmann's formulation (Gassmann, 1951) and the effects of the effective stresses with Hertz-Mindlin's relation (Mindlin, 1949).

## 2 SEISMIC MODELLING

The reservoir model was included into a 1D-model, constructed with the data of the sonic log available from the surface to far below the reservoir zone. Densities were estimated using Gardner's empirical relation between densities and *P*-wave velocities (Gardner *et al.*, 1974). The *S*-wave velocities were estimated using a  $V_P/V_S$  ratio of 1.8 in the carbonate reservoirs and a velocity ratio of 2 in the overburden.

### 2.1 Post-Stack Modelling

Wave propagation was simulated by ray tracing at each time lapse step, over a maximum offset of 1600 m. The simulated records were convolved by a 60 Hz central frequency Ricker and stacked in order to get time-lapse sections at a few spatial positions. One of these time-lapse sections, showing the stacked traces recorded over the period of injection at the same point, is displayed on the left of Figure 4, while the difference section obtained by subtracting the pre-injection trace from the stacked traces at each step is displayed on the right.

A clear marker is visible on the time lapse difference section, at the top of the uppermost reservoir. At the early

### 2.2 Pre-Stack Modelling

#### 2.2.1 AVO Effects

The amplitude of the *P*-wave reflection at the top of the uppermost reservoir varies with the wave front incidence angle,  $\theta_i$ , according to Zoeppritz equations (Fig. 5).

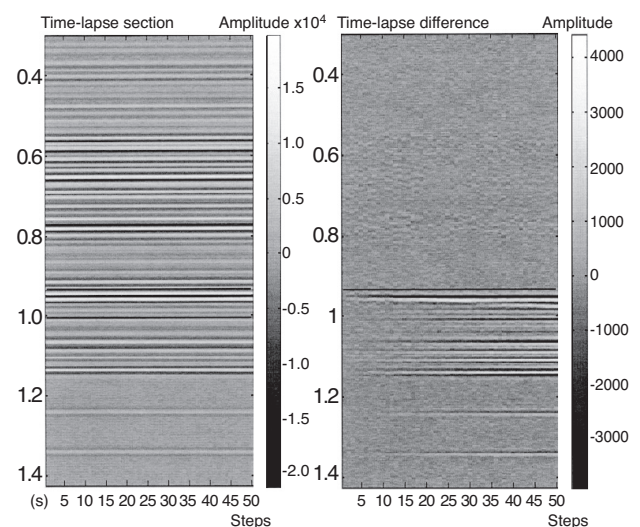


Figure 4  
Time-lapse seismic section and difference with the pre-injection trace.

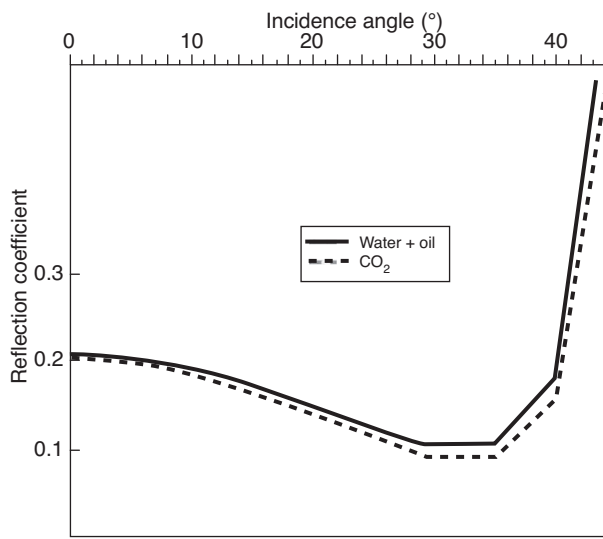


Figure 5

Amplitude *versus* incidence angle at the top of the uppermost reservoir computed with Zoeppritz equation.

With the velocities given by the sonic log at the first well and the estimated values of the fluid bulk modulus, the difference in amplitude is about 2.5% at zero offset (reflection coefficients of 0.216 before  $\text{CO}_2$  injection, 0.211 when  $\text{CO}_2$  is present), 5% for a  $20^\circ$  incidence (0.154 and 0.146 respectively) and about 10% for an incidence ranging from 30 to  $35^\circ$ , *i.e.* for offsets from 1000 to 1450 m. The reflection coefficients are 0.105 before the injection and 0.0945 in the presence of gas.

The amplitude variation at offsets between 1000 and 1400 m could be at the limit of the measurement capabilities, provided the signal-to-noise ratio can be kept at a sufficient level.

## 2.2.2 Elastic Modelling

A simulation based on the wave equation, was performed using a 1D-model, built with the sonic data recorded in the most documented well. The reflection at the top of the reservoir, at about 780 ms, is overlaid, at mid-offset traces, by strong events, generated by  $P$  to  $S$  conversion at the interface of upper layers with a high contrast in acoustic impedances (*Fig. 6*).

The presence of a low velocity layer near the surface, which the model does not take into account, would probably horizontalize the wavefront near the surface and reduce the amplitude of the projection of the converted waves onto the vertical component. However, filtering these  $P$ - $S$  reflections might be an issue. Three-component recording could perhaps help to separate the waves.

## 3 FRACTURATION EFFECTS

The simulations shown until now used velocities computed with Gassmann's formula that was developed for isotropic homogeneous porous rocks. In the case of the site under study, the discrepancy between the permeability measured on cores and the permeability inferred from well tests suggest that fractures or cracks play an important role in fluid flows in the reservoir.

Due to the weight of the overlying rocks, cracks and fractures generally organize in one or a few vertical sets, thus inducing an azimuthal anisotropy, the seismic waves propagating with different velocities according to the angle between the direction of propagation and the main vertical set of cracks or fractures.

### 3.1 Modelling Fractured Rocks

Several models have been proposed to describe fractured media and allow computation of the mechanical effects of a seismic perturbation. In the "penny-shape" model, cracks are represented by thin ellipsoids with a circular vertical base (Hudson, 1981) and the fractured medium is characterized by a "crack density",  $d_c$ . In the "linear slip model", fractures are modelled by long thin parallel planes and the fractured medium is characterized by its vertical and tangential compliances,  $\Delta_N$  and  $\Delta_T$  (Schoenberg and Douma, 1988).

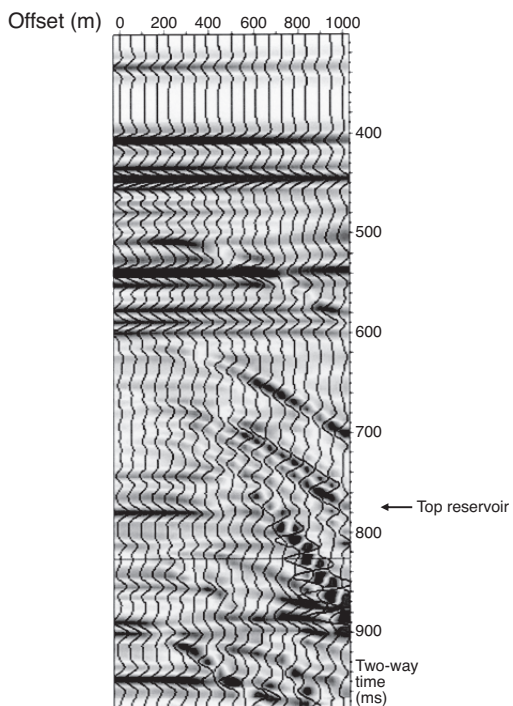


Figure 6  
Elastic seismic shot modelling.

For an isotropic background medium, both models lead to an anisotropy with a horizontal symmetry axis, described as “Horizontal Transverse Isotropy” (HTI). The same anisotropy parameters can be related to one model or to the other, so that characterizing the anisotropy gives no information about the shape and size of the cracks or fractures.

### 3.2 Fluid Factor

Both models consider independent fractures, with no relation with the background porous medium. For independent isolated fractures, normal relative motions of the crack or fracture faces were considered possible when the fractures were filled with compressible gases and not totally impossible when the cracks were filled with a rather uncompressible fluid as water or oil. As the liquids filling the fractures are liable to flow into the porous system, the relations between the porous medium and the fractures must be taken into account (Thomsen, 1995). The discontinuity of normal displacement through liquid-filled fractures or cracks is then a fraction of the discontinuity computed for dry or gas-filled cracks. This fraction, the fluid factor, is a function of the fluid bulk modulus, of the crack and pore porosities and of the mechanical properties of the grains. The fluid factor ( $F_{fl}$ ) is close to 1 for gases and has values between 0 and 1 for less compressible fluids.

### 3.3 Azimuthal Anisotropy

The mechanical behaviour of a HTI medium can be characterized by the vertical  $P$  and  $S$ -wave velocities and by three anisotropy parameters,  $\epsilon^{(v)}$ ,  $\delta^{(v)}$  and  $\gamma^{(v)}$ . These parameters can be expressed as a function of the adimensional normal and tangential compliances as (Bakulin *et al.*, 2000):

$$\begin{aligned}\epsilon^{(v)} &= -2g(1-g)\Delta_N, \\ \delta^{(v)} &= -2g[(1-2g)\Delta_N + \Delta_T], \\ \gamma^{(v)} &= -\frac{\Delta_T}{2} \\ \text{where } g &= \left(\frac{V_S}{V_P}\right)^2\end{aligned}$$

We shall express the anisotropy parameters as functions of the shear-wave splitting parameter  $\gamma$ , which can be measured in accessible wells by sonic logs. The value of the shear-wave splitting parameter is close to the penny-shape model’s crack density and is half the tangential compliance of the linear slip model.

Equivalence of the penny-shape and “linear slip” models for the description of a HTI model yields:

$$\Delta_T = \frac{16d_c}{3(3-2g)} \text{ and } \Delta_N = \frac{4d_c}{3g(1-g)} = \frac{3-2g}{2g(1-g)} F_{fl} \gamma$$

The anisotropy parameters can then be expressed as a function of the shear-wave splitting parameter and of the fluid factor:

$$\begin{aligned}\epsilon^{(v)} &= -(3-2g)F_{fl}\gamma, \\ \delta^{(v)} &= -\left[\frac{(3-2g)(1-2g)}{1-g} F_{fl} + 4g\right]\gamma, \\ \gamma^{(v)} &= -\gamma\end{aligned}$$

In an azimuthal anisotropic medium, the horizontal velocities are a function of the angle between the propagation direction and the symmetry axis. The seismically measurable effects are a variation in the normal moveout or NMO velocities, utilized in the stacking process, and a variation of the reflection coefficients with the azimuth.

The decametric thicknesses of the reservoirs are too small to allow an accurate measure of the NMO velocities. On the contrary, variations of the amplitude with the incidence angle might be measurable and give information about the fracture nets and their relation to the pores.

#### 3.3.1 Amplitude Versus Offset and Azimuth

An approximation of the Zoeppritz equations describing the dependence of the amplitude of the reflection at an interface to the incidence angle has been given for isotropic media (Aki and Richards, 1980):

$$R_p(m) = \frac{\Delta I_p}{2I_p} + \frac{1}{2} \left\{ \frac{\Delta V_p}{\bar{V}_p} - 8\bar{g} \frac{\Delta \mu}{\mu} \right\} \sin^2 m + \frac{\Delta V_p}{2\bar{V}_p} \sin^2 m \tan^2 m$$

where the  $\Delta$  indicates the difference and the upper bar the average of the values across the interface,  $\bar{g}$  notes the squared ratio of the average  $S$  and  $P$  velocities, and  $m$  is the average of the incidence and transmission angles.

This relation is valid when the wave propagates in a plane perpendicular to the symmetry axis, *i.e.* in the direction of the principal fracture net.

For waves propagating in a plane perpendicular to the main fracture system, an additional term, function of the anisotropy parameters is added (Rüger, 1998):

$$\begin{aligned}\delta R_p &= R_p(m, 0) - R_p\left(m, \frac{\pi}{2}\right) = \\ &\quad \left[ 4\bar{g}\Delta\gamma + \frac{\Delta\delta^{(v)}}{2} \right] \sin^2 m + \frac{\Delta\epsilon^{(v)}}{2} \sin^2 m \tan^2 m\end{aligned}$$

If we can consider the seal as practically isotropic, we may express this difference as:

$$\begin{aligned}\delta R_p &= \left[ 2(2\bar{g} - g) - \frac{(3-2g)(1-2g)}{2(1-g)} F_{fl} \right] \times \\ &\quad \gamma \sin^2 m - \frac{3-2g}{2} F_{fl} \gamma \sin^2 m \tan^2 m\end{aligned}$$

The  $V_p/V_s$  ratio is close to 1.83 in the limestone reservoir and  $g$  is close to 0.3. The value of the  $V_p/V_s$  ratio is about 2.1 in the sealing shales, so that the square of the ratio of the average of  $S$ - and  $P$  velocities across the interface has a value of about 0.27. The difference between the reflection coefficients at a given incidence angle along the two principal horizontal anisotropy axes is:

$$0.48 \left[ 1 - \frac{10}{7} F_{fl} \right] \gamma \sin^2 m - 1.2 F_{fl} \gamma \sin^2 m \tan^2 m$$

For the reservoir under study, with a mean porosity of 8.5% and water and oil in equal proportion in the pores, the fluid factor can be estimated at 0.83.

For such a value, the factor of  $\sin^2 m$ , known as the AVO “gradient”, is small and will hardly be measurable.

The second term of the azimuthal AVO difference, measurable at large incidence angles, gives an estimation of the product  $F_{fl} \gamma$ . When  $\text{CO}_2$  is present in the pores and the fluid factor is close to 1, an estimation of  $\gamma$  alone is possible.

A simulation of the amplitude variations in the two principal horizontal directions of anisotropy was performed, using a rough estimate of the unknown shear-wave splitting parameter at 0.1, inferred from the values measured in the same level in another field of the south-eastern Paris Basin, where the influence of fractures on fluid flows seemed quasi similar (Li *et al.*, 1995).

Figure 7 shows the variation of the reflection coefficients with the square of the sine of the incidence angle in the two principal horizontal directions of anisotropy in the cases when cracks or fractures are filled with oil and water and when they also contain  $\text{CO}_2$ . The slope at low incidence angles is the AVO gradient. The deviations to the low incidence slope at large incidence angles are proportional to the product  $F_{fl} \gamma$  of the fluid factor by the shear wave splitting parameter.

The difference between the reflection coefficients due to the substitution of  $\text{CO}_2$  to brine is slightly larger in the direction perpendicular to the main fracture direction than in the direction of fracturation (0.04 and -26% against 0.03 and -16% at an incidence angle of 30°, for which  $\sin^2 m \sim 0.4$ ).

The difference between the reflection coefficients in the direction of the main set of fractures and in the perpendicular direction is 0.03 in the case of liquid filling and 0.04 when  $\text{CO}_2$  is present, representing a variation of 17 and 28%, respectively, at an incidence angle of 30°.

Product  $F_{fl} \gamma$  can be estimated from the deviations of the curves from the low incidence slopes. The two terms of the product can then be separated in the zones reached by the  $\text{CO}_2$  plume when both pre-injection and while-injection data are available.

The  $F_{fl} \gamma$  product, which may vary spatially, is probably related to the flow properties in the storage, being related both to the density of cracks and fractures and to the connection between the cracks or fractures and pores.

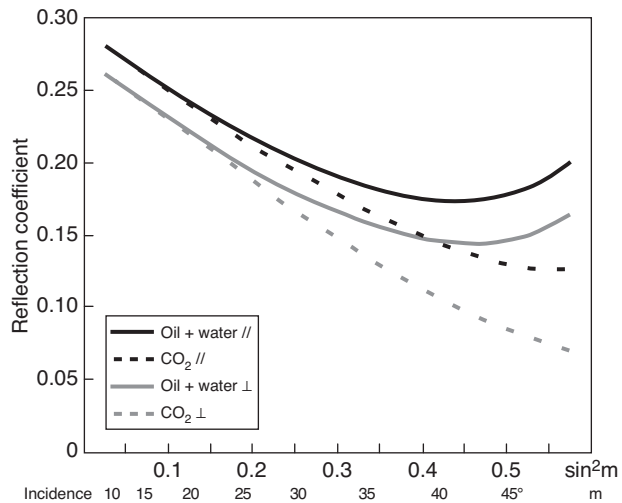


Figure 7  
Amplitude versus incidence angle for the  $P-P$  reflection at the top of the reservoir.

Being able to measure the dip of the amplitude differences with a sufficient accuracy implies that the reflections at the top of the storage are not overlaid by reflections from reflectors above. Three-component acquisition might help to attenuate the converted waves overlying the storage top reflection at large incidences.

### 3.3.2 $P-S$ Reflections

3-C acquisition will also give access to converted  $P-S$  reflections.

The  $P-S$  reflection coefficient in the direction of the fractures can be computed as a function of the contrasts in density and velocity across the interface (Aki and Richards, 1980). This function is approximately proportional, at small offsets, to the sine of the incidence angle.

Owing to the high contrast in  $S$ -wave velocities between the sealing shales and the limestone reservoir, the converted waves become rapidly perceptible, the converted reflection coefficient reaching -0.12 at a 10° incidence angle and -0.22 at 20°, with a gradient equal to -0.73.

The difference between the  $P-S$  AVO gradients in the two principal horizontal directions of anisotropy has been given as a function of the normal and tangential adimensional compliances (Bakulin *et al.*, 2000), as:

$$\frac{1}{1 + \sqrt{g}} \left[ \sqrt{g} \Delta_Y - g(1 - 2g) \Delta_N \right]$$

which can be written as a function of the shear-wave splitting parameter and of the fluid factor:

$$\frac{1}{1 + \sqrt{g}} \left[ 2\sqrt{g} - \frac{(3 - 2g)(1 - 2g)}{2(1 - g)} F_{fl} \right] \gamma$$

with  $g = 0.3$ , this expression is close to  $(0.7 - 0.44 F_{fl}) \gamma$ .

With a shear-wave splitting parameter equal to 0.1, the differences between the *P-S* AVO gradients in the two horizontal principal directions of anisotropy are 0.033 for the initial water and oil filling and 0.026 when CO<sub>2</sub> is present in the pores, *i.e.* 5 and 4% of the gradient in the direction of cracks or fractures. These differences are probably too small to be measured.

## CONCLUSION

In the case of the carbonate reservoir under study, the seismically measurable effects of carbon dioxide replacing the oil/water mixture in the pores of the reservoir will consist in a slight but detectable time shift for reflections happening beneath the reservoir and in a difference in the amplitude of the reflection at the reservoir level, which may reach some 10% and might be detectable and measurable.

The amplitude variations due to the fluid substitution are greater at large incidence angles, but picking and accurately measuring the reflection at the top of the storage will probably not be straightforward, because of the presence of converted events from overlying reflectors

Some information about the permeability might be extracted from differences in the AVO curves in the direction of the principal fracture net and in the perpendicular direction.

However, all the effects related to the fluid substitution are small and their measurement will necessitate careful acquisition and data processing.

## ACKNOWLEDGMENTS

This work was supported by funding of the French National Research Agency in the frame of the Géocarbone-monitoring project.

## REFERENCES

- Aki K.I., Richards P.G. (1980) *Quantitative seismology*, W.H. Freeman and Co, New York.
- Bakulin A., Grechka V., Tsvankin I. (2000) Estimation of fracture parameters from reflection seismic data – Part I: HTI model due to a single fracture set, *Geophysics* **65**, 1788-1802.
- Gardner G.H.F., Gardner L.W., Gregory A.R. (1974) Formation velocity and density. The diagnostic basis for stratigraphic traps, *Geophysics* **39**, 770-780.
- Gassmann F. (1951) Über die Elastizität poröser Medien, *Vierteljahrsschrift. der NaturForschenden Gesellschaft in Zurich* **96**, 1-23.
- Hudson J.A. (1981) Wave speeds and attenuation of elastic waves in material containing cracks, *Geophys. J. R. Astr. Soc.* **64**, 133-150.
- Li X.Y., MacBeth C., Lefevre F., Tabti H. (1995) Characterizing fractured reservoir by multicomponent reflection data and VSPs in the Paris Basin, *65th SEG Meeting*, IN3.4, 344-347.
- Mindlin R.D. (1949) Compliance of elastic bodies in contact, *J. Appl. Mech.* **16**, 259.
- Rüger A. (1998) Variation of P-wave reflectivity with offset and azimuth in anisotropic media, *Geophysics* **63**, 935-947.
- Schoenberg M., Douma J. (1988) Elastic wave propagation in media with parallel fractures and aligned cracks, *Geophys. Prospect.* **36**, 571-590.
- Thomsen L. (1995) Elastic anisotropy due to aligned cracks in porous rocks, *Geophys. Prospect.* **43**, 805-829.

*Final manuscript received in June 2009  
Published online in September 2009*

Copyright © 2009 Institut français du pétrole

Permission to make digital or hard copies of part or all of this work for personal or classroom use is granted without fee provided that copies are not made or distributed for profit or commercial advantage and that copies bear this notice and the full citation on the first page. Copyrights for components of this work owned by others than IFP must be honored. Abstracting with credit is permitted. To copy otherwise, to republish, to post on servers, or to redistribute to lists, requires prior specific permission and/or a fee: Request permission from Documentation, Institut français du pétrole, fax. +33 1 47 52 70 78, or [revueogst@ifp.fr](mailto:revueogst@ifp.fr).